Modal Analysis of the Directivity of Acoustic Emissions from Wavepackets in Turbulent Jets

Conference Paper · January 2020

DOI: 10.2514/6.2020-0745

2 authors:

Akhil Nekkanti
University of California, San Diego
18 PUBLICATIONS **129** CITATIONS

SEE PROFILE

Oliver T. Schmidt
University of California, San Diego
83 PUBLICATIONS **2,883** CITATIONS

SEE PROFILE

AIAA SciTech Forum
6-10 January 2020, Orlando, FL
AIAA Scitech 2020 Forum

10.2514/6.2020-0745

Modal Analysis of the Directivity of Acoustic Emissions from Wavepackets in Turbulent Jets

Akhil Nekkanti * and Oliver T. Schmidt †
University of California San Diego, La Jolla, CA, 92093, USA

The directivity of noise from three large-eddy simulations of turbulent jets at Mach 0.7, 0.9 and 1.5 and the first three azimuthal wavenumbers is investigated using spectral proper orthogonal decomposition (SPOD). First, a weighting function for the pressure 2-norm that is localized to the far-field is employed to educe the overall most energetic radiation patterns. Second, we isolate radiation patterns to specific jet inlet angles by restricting the spatial weighting to small rectangular regions in the far-field. The most energetic radiation pattern for all cases and relevant frequencies is a single superdirective acoustic beam in the downstream direction. The source region of these beams is traced back to the end of the potential core for low frequencies and the shear-layer region for higher frequencies. In the sideline direction to low angles, the acoustic patterns consist of waves that propagate upstream or perpendicular to the jet axis. The sideline radiation patterns are found to originate from the same source locations as the dominant superdirective beams. Inspection of the SPOD modes reveals that sideline radiation is directly slaved to directive downstream radiation. These results indicate that large-scale coherent structures are the dominant source of acoustic radiation to all the angles.

I. Nomenclature

ρ	=	Density
μ	=	Dynamic viscosity
f	=	Frequency
p	=	Pressure
c	=	Speed of sound
t	=	Time
x_c	=	Length of the potential core
$\psi_{f_k}^{(j)}$	=	j-th SPOD mode at k-th frequency
$\lambda_{f_k}^{(j)}$	=	Eigenvalue of the j-th mode at k-th frequency
W	=	Weight matrix
Re	=	Reynolds number
m	=	Azimuthal wavenumber
D	=	Nozzle diameter
M_j	=	Jet Mach number
ϕ	=	Jet inlet angle. Angle with respect to the upstream jet axis (negative x-axis)
T	=	Temperature
Ω	=	Computational domain: $x, r \in [0, 30] \times [0, 6]$
U	=	Axial velocity
St	=	Jet Strouhal number fD/U_j
$St_{\max}$	=	Maximum Strouhal number of the post processing

Subscripts

j	=	Nozzle exit
∞	=	Ambience

*Graduate Student, Department of Mechanical and Aerospace Engineering
†Assistant Professor, Department of Mechanical and Aerospace Engineering, AIAA Member

II. Introduction

The reduction of jet noise is an important objective for the aviation community. The pioneering works by Crow and Champagne [1] and Brown and Roshko [2] were the earliest to report the presence of large-scale coherent structures in turbulent jets and shear layers, respectively. Mollo-Christensen [3] described them as intermittent spatial structures, or wavepackets, present in the mixing layer. Researchers [4–8] have modeled the coherent structures as growing and decaying instability waves of the turbulent mean flow. These wavepackets were identified as the main source of aft-angle noise [9]. The acoustic radiation of wavepackets is highly directive and concentrated in the downstream direction. The directive emission shows an exponential decay at high polar angles θ, or low jet inlet angle angles $\phi = 2\pi - \theta$, correspondingly. This pattern was termed superdirective radiation by Crighton and Huerre [8]. In this work, we will use this word more loosely and refer to radiation patterns that are isolated and clearly directed downstream as superdirective. Cavalieri et al. [10] have shown that the axisymmetric mode of the subsonic jets exhibit super-directivity. Readers can refer to Jordan and Colonius [9] for a comprehensive review on wavepackets in turbulent jets.

Based on experimental observations and the author's physical interpretation of the source mechanisms, Tam et al. [11] proposed a separation of the far-field spectrum into two similarity spectra for the downstream and sideline radiation, respectively. The wavepacket-generated radiation in the downstream direction is modelled by the large-scale similarity (LSS) spectrum and a fine-scale similarity (FSS) spectrum is proposed for the sideline radiation. This approach was later extended to subsonic jets by Viswanathan [12, 13] and Tam et al. [14].

Wavepackets have been studied extensively using various approaches such as global linear stability analysis [15], parabolized stability equations [16–18], resolvent analysis [19–23], spectral proper orthogonal decomposition [21, 24, 25] and one-way Navier-Strokes equations (OWNS) [26]. Nichols and Lele [15] used global linear theory to predict the Kelvin-Helmholtz instability waves and the instability waves predicted by Tam and Hu [27]. Schmidt et al. [24] used SPOD and global stability theory to extract and predict both downstream and sideline radiation patterns. Rigas et al. [26] computed the wave patterns of the downstream radiation using OWNS equations. A conditional space-time proper orthogonal decomposition was formulated by Schmidt and Schmid [28] to statistically characterize the evolution of acoustic bursts. Trapped acoustic modes in the potential core were identified and analyzed in detail by Towne et al. [29] and by Schmidt et al. [30]. The jet noise in sideline direction is commonly associated with fine-scale turbulence. Recent numerical studies [22–24, 31], strongly suggest that large-scale coherent structures also play an important role in that regard. Papamoschou [31] used a stochastic extension of analytical wavepacket models to show that the far-field noise at both low and high angles can be explained by a single source mechanism. Results by Schmidt et al. [24] and Jeun and Nichols [22] obtained using linear global stability and resolvent analysis, respectively, underpin the notion that large-scale coherent structures may significantly contribute to the sideline radiation. We provide further empirical evidence for this hypothesis by applying spectral proper orthogonal decomposition to educe directional noise.

Modal decomposition techniques [32, 33] facilitate the analysis of complex flows by extracting essential features. The most widely used approach, proper orthogonal decomposition (POD), was introduced by Lumley [34, 35] to educe coherent structures from turbulent flow fields. Space-only POD computed using the method of snapshots was later introduced by Sirovich [36] and is the most commonly used form of POD. It decomposes the flow field into temporal coefficients and spatial modes that optimally represent the data in terms of energy. The temporal POD expansion coefficients contain, in general, a combination of different time scales and are only correlated at zero time lag. Spectral proper orthogonal decomposition (SPOD) is the frequency-domain variant of POD. It computes modes that oscillate at a single frequency from statistically stationary data. By construction, SPOD identifies structures that are coherent in both space and time [25] (in the strict mathematical sense). A number of studies showed that the dominant dynamics are often accurately captured by only a few modes [21, 25, 37–39]. Experimentally, Glauser et al. [37], Citriniti and George [38] and Jung et al. [39] showed that a large fraction of the kinetic energy is contained in the first three SPOD modes. Recently, Schmidt et al. [21] applied SPOD to high-fidelity simulation data of turbulent jets in the subsonic, transonic, and supersonic regimes. The authors give a detailed account of the Kelvin-Helmholtz and the Orr-type instability mechanisms that dominate the initial shear-layer and the region downstream of the potential core, respectively. Towne et al. [25] performed SPOD on Mach 0.4 turbulent jet and present a detailed account of the method and its relationship to space-only POD, resolvent analysis, and dynamic mode decomposition (DMD).

In the present study, we perform SPOD of LES simulation data of jets at Mach 0.7, 0.9 and 1.5, and analyze radiation wave patterns with special emphasis on directivity. The remainder of this paper is arranged as follows. In section III, the methodology is recapitulated. In section IV, the results are presented and the work is summarized in section V.

III. Spectral Proper Orthogonal Decomposition

SPOD computes monochromatic modes that are optimally ranked by energy. Due to the optimality and coherence properties, SPOD modes often represent the dynamically most relevant and prevailing flow structures. Given a flow field $\mathbf{q}_i = \mathbf{q}(t_i) \in \mathbb{C}^n$, where $\mathbf{q}$ represents a wide-sense stationary process that is sampled at n_t discrete time instances $t_1, t_2, ..., t_{n_t}$, the data matrix $\mathbf{Q}$ of the fluctuating field is defined as

$$\mathbf{Q} = \left[\mathbf{q}_1 - \bar{\mathbf{q}}, \mathbf{q}_2 - \bar{\mathbf{q}}, ..., \mathbf{q}_{n_t} - \bar{\mathbf{q}}\right] \in \mathbb{C}^{n \times n_t}. \tag{1}$$

Here, $\bar{\mathbf{q}}$ denotes the temporal mean. The instantaneous energy $\|\mathbf{q}\|_x^2 = \langle \mathbf{q}, \mathbf{q} \rangle_x$ of a given quantity may be expressed in terms of a spatial inner product

$$\left\langle \mathbf{q}, \mathbf{q} \right\rangle_x = \int_\Omega \mathbf{q}^*(x', t) \mathbf{W}(x') \mathbf{q}(x', t) dx', \tag{2}$$

where $\mathbf{W}$ is a weight matrix that accounts for numerical quadrature and component-wise weights. $(.)^*$ denotes the complex conjugate. Analogously, the total energy of the quantity is defined via the corresponding space-time inner product

$$\left\langle \mathbf{q}, \mathbf{q} \right\rangle_{x,t} = \int_{-\infty}^{\infty} \int_\Omega \mathbf{q}^*(x', t) \mathbf{W}(x') \mathbf{q}(x', t) \mathrm{d}x' \mathrm{d}t. \tag{3}$$

To estimate the cross-spectral density, we use Welch's [40] approach and segment the data into n_{blk} overlapping blocks. The l-th block,

$$\mathbf{Q}^{(l)} = \left[\mathbf{q}_1^{(l)} - \bar{\mathbf{q}}, \mathbf{q}_2^{(l)} - \bar{\mathbf{q}}, \cdots, \mathbf{q}_{n_{\mathrm{freq}}}^{(l)} - \bar{\mathbf{q}}\right] \in \mathbb{C}^{n \times n_{\mathrm{freq}}} \tag{4}$$

contains n_{freq} snapshots as its columns. Each block is considered a statistically independent realization under the ergodic hypothesis. Next, the row-wise discrete Fourier transform is performed on each block to yield

$$\hat{\mathbf{Q}}^{(l)} = \left[\hat{\mathbf{q}}_1^{(l)}, \hat{\mathbf{q}}_2^{(l)}, ..., \hat{\mathbf{q}}_{n_{\mathrm{freq}}}^{(l)}\right] \in \mathbb{C}^{n \times n_{\mathrm{freq}}}. \tag{5}$$

By $\hat{\mathbf{q}}_i^l$ we denote the l-th Fourier realization at i-th discrete frequency. We proceed by arranging all Fourier realizations at a fixed frequency f_k in a matrix

$$\hat{\mathbf{Q}}_{f_k} = \left[\hat{\mathbf{q}}_{f_k}^{(1)}, \hat{\mathbf{q}}_{f_k}^{(2)}, ..., \hat{\mathbf{q}}_{f_k}^{(n_{\mathrm{blk}})}\right] \in \mathbb{C}^{n \times n_{\mathrm{blk}}}. \tag{6}$$

The cross-spectral density matrix at each frequency is then calculated as

$$\mathbf{S}_{f_k} = \hat{\mathbf{Q}}_{f_k} \hat{\mathbf{Q}}_{f_k}^* \in \mathbb{C}^{n \times n}. \tag{7}$$

The eigenvalue decomposition of the cross-spectral density matrix,

$$\mathbf{S}_{f_k} \mathbf{W} \mathbf{\Psi}_{f_k} = \mathbf{\Psi}_{f_k} \mathbf{\Lambda}_{f_k}, \tag{8}$$

yields the SPOD modes, $\mathbf{\Psi}(x)$. The mode energies are the corresponding eigenvalues on the diagonal of $\mathbf{\Lambda}_{f_k} = diag\left(\lambda_{f_k}^{(1)}, \lambda_{f_k}^{(2)}, ...\lambda_{f_k}^{(n)}\right)$, where $\lambda_{f_k}^{(1)} \geq \lambda_{f_k}^{(2)} \geq ... \geq \lambda_{f_k}^{(n)}$. The first SPOD mode contains the largest fraction of the total energy at each frequency and is often referred as the leading or optimal mode. Subsequent modes are referred to as suboptimal modes. The SPOD modes are orthogonal at the same frequency, i.e.,

$$\mathbf{\Psi}_{f_k}^* \mathbf{W} \mathbf{\Psi}_{f_k} = \mathbf{I} \in \mathbb{R}^{n_{\mathrm{blk}} \times n_{\mathrm{blk}}}, \tag{9}$$

where $\mathbf{I}$ is the identity matrix. The ability of SPOD to decouple the dynamics from different time scales makes the results highly interpretable.

IV. Results and Discussions

We analyse the large-eddy simulations (LES) databases of turbulent jets at Mach numbers $M_j = 0.7$, 0.9 and 1.5 computed by Brès et al. in [41], [42], and [43], respectively. The reader is referred to Brès et al. [41–43] for further details on the numerical method and meshing strategy. The flow is non-dimensionalized by the nozzle exit values, namely, velocity by U_j, pressure by $\rho_j U_j^2$, length by the nozzle diameter D, and time by D/U_j. Frequencies are reported in terms of the Strouhal number $St = fD/U_j$. A cylindrical domain Ω of size $x, r \in [0, 30] \times [0, 6]$ is used for the

Table 1 Parameters of the Large-Eddy Simulations

case	Re	M_j	T_j/T_∞	p_0/p_∞	$\Delta t c_\infty/D$	$St_{\max}$	Reference
Supersonic	1.55×10^5	1.5	1.74	3.67	0.1	1.0	case A2 [43]
Transonic	1.01×10^6	0.9	1.0	1.7	0.2	1.6	[42]
Subsonic	0.79×10^6	0.7	1.0	1.4	0.2	1.6	[41]

analysis. The LES data consists of 10,000 snapshots separated by a time step of $\Delta t c_\infty/D$. Important parameters are summarized in table 1.

Previous studies [9, 10, 44–46] have reported that most of the far-field sound energy is concentrated in the first three azimuthal wavenumbers, $m = 0, 1$ and 2. For the sound radiated in the downstream direction, the axisymmetric mode ($m = 0$) is most dominant, while the helical ($m = 1$) and the double-helical modes ($m = 2$) become more important in the sideline direction [9]. In this study, we focus our attention on the noise emitted by these three azimuthal wavenumbers. The directivity of the radiation is expressed in terms of the jet inlet angle ϕ, defined with respect to the negative x-axis, such that 180° corresponds to the downstream direction and 90° to the sideline direction perpendicular to the jet axis. The sound radiated to the far-field is computed by calculating the overall sound pressure level (OASPL) along the upper boundary at $r = 6$. The power spectral density (PSD) and the OASPL are defined as

$$\mathrm{PSD} = 10\log_{10}\left(\frac{\hat{p}'(m,\phi,St)\hat{p}'^{*}(m,\phi,St)}{p_{\mathrm{ref}}^2 St_{\min}}\right), \quad \text{and} \tag{10}$$

$$\mathrm{OASPL} = 10\log_{10}\left(\sum_{St_{\min}}^{St_{\max}}\frac{\hat{p}'(m,\phi,St)\hat{p}'^{*}(m,\phi,St)}{p_{\mathrm{ref}}^2}\right), \tag{11}$$

respectively. Here, p_{ref} is the reference pressure and $\hat{p}'$ is the Fourier transform of the pressure fluctuations in time.

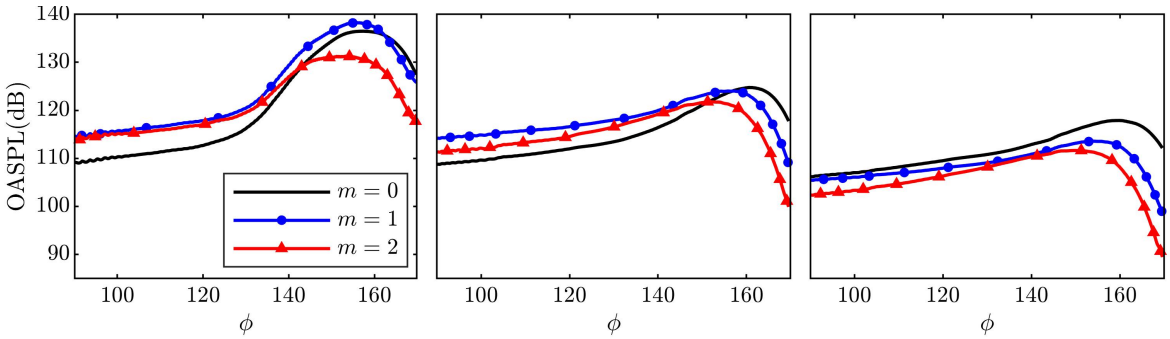

(a) Supersonic Jet $M_j = 1.5$ **(b) Transonic Jet $M_j = 0.9$** **(c) Subsonic Jet $M_j = 0.7$**

Fig. 1 Overall sound pressure level at different jet inlet angles; OASPL for $m = 0$ (black solid lines), $m = 1$ (blue lines with circles) and $m = 2$ (red lines with triangles).

The PSD is estimated using the Welch's method [40] with 50% overlap and $n_{\mathrm{freq}} = 512$. Within the radial extent of the computational domain ($r \leq 6$) and at high jet inlet angles, the hydrodynamic component contributes a significant part of the energy associated with pressure fluctuations [47]. To eliminate the effect of the hydrodynamic component, a high-pass filter ($St \geq 0.1$) based on SPOD reconstruction [48] is used. The OASPL of the filtered signals for different azimuthal wavenumbers and different Mach numbers are presented are presented in Fig. 1. The overall sound pressure level at each ϕ is a measure of the total sound radiated in that particular direction. The OASPL of azimuthal mode $m = 1$ peaks at $\phi = 156°$ for the supersonic jet, whereas the $m = 0$ component peaks at $\phi = 162°$ for the transonic and subsonic jets. These angles are in agreement with the observations made by Jordan and Colonius [9] and Tam et al. [14]. For the supersonic jet, the $m = 1$ component dominates at most angles. At lower inlet angles, $m = 2$ is the leading subdominant component. At higher angles, this component is replaced by $m = 0$. In the case of the transonic jet, $m = 1$ is the most dominant component in the range $90° \leq \phi \leq 155°$, whereas $m = 0$ is the most dominant component for

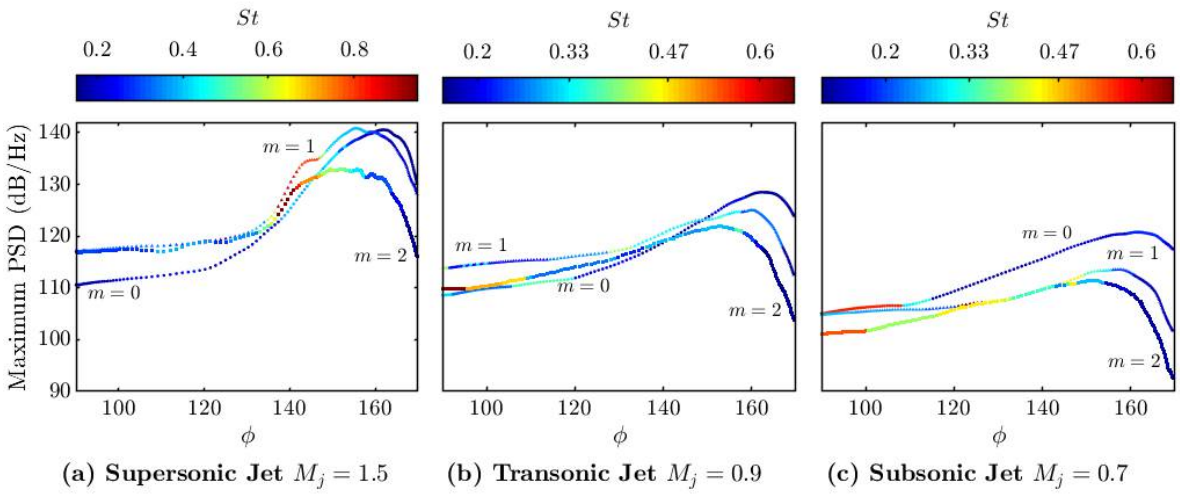

Fig. 2 Maximum PSD as a function of jet inlet angle: $m = 0$, $m = 1$ and $m = 2$. False colors indicate corresponding peak frequency.

$\phi \geq 155°$. For subsonic jets, the OASPL curves in Fig. 1(c) show that, $m = 0$ is clearly the most dominant mode, followed by $m = 1$ and then $m = 2$. For all the three jets, the $m = 1$ component is larger than the $m = 2$ contribution. With increasing azimuthal wavenumber, the peak OASPL shifts towards lower jet inlet angles.

The scatter plot in Fig. 2 shows the variation of the maximum PSD as a function of the jet inlet angle. False colors show the corresponding Strouhal number. Similar trends as for the OASPL are observed, see Fig. 1. The false color indicates the frequency with the largest contribution to the PSD at each angle. It can be seen that the frequency of the peak PSD is $St = 0.4$ for the supersonic case and $St = 0.2$ for the transonic and subsonic cases, respectively. In particular for the supersonic jet, it is observed that lobes in the PSD at high jet angle correspond to distinct frequency bands. In all three cases, the axisymmetric azimuthal component peaks at $\phi \approx 160°$ and $St \approx 0.2$. The presence of discrete color bands in Fig. 2 suggests a clear relationship between radiation angle and frequency.

The SPOD eigenvalues and modes are computed for the pressure. The pressure 2-norm is used as a proxy of the acoustic energy in the far-field. To isolate contributions to the far-field, we choose a weighting function

$$W(x) = \begin{cases} 1 & \text{for } 5 \leq r \leq 6, \forall x \in \Omega \\ 0 & \text{otherwise.} \end{cases} \tag{12}$$

Fig. 3 shows the SPOD spectra for all cases and azimuthal wavenumbers under consideration. Below St = 0.1, the far-field pressure partially consists of hydrodynamic fluctuations. As we are interested in acoustics, we omit this region for clarity. Parts of some of the spectra exhibit a large difference between the first (optimal, or leading) and second (first suboptimal) modes. This behavior is referred to as low-rank behavior [21] and indicates dominance of a physical mechanism associated with the first mode. It is most pronounced for the axisymmetric component within the ranges $0.1 \leq St \leq 0.6$ and $0.1 \leq St \leq 0.7$ for the transonic and subsonic jets, respectively. The prevalence of this behavior decreases as m increases. The frequency at which the low-rank behavior peaks is termed as the dominant frequency. Modes at representative frequencies and azimuthal wavenumbers are shown in Fig. 4. In particular, we pick the maximum OASPL azimuthal wavenumber, see Fig. 1. The SPOD modes clearly indicate the dominance of superdirective acoustic radiation emanating from the end of the potential core as the main source of high inlet-angle jet noise.

The radiation patterns confirm the relationship between the jet inlet angle and frequency previously discussed in the context of Fig. 2. The source of the superdirective radiation is the Kelvin-Helmholtz (KH) wavepackets, i.e. the instability of the annular jet shear-layer [21, 26]. Directive beams that propagate at steeper angles are observable at the higher frequencies of $St = 0.6$ and $St = 1.0$ (middle and bottom row Fig. 4). The first, second, and third sub-optimal modes at $St = 0.6$ are shown in Fig. 5. Multiple directive beams are observed for all the jets. The number of beams increases with mode number. The suboptimal mode of the transonic and subsonic jets exhibit two superdirective beams. These beams originate from either side of the end of the potential core. Rigas et al. [26] suggest that these two beams

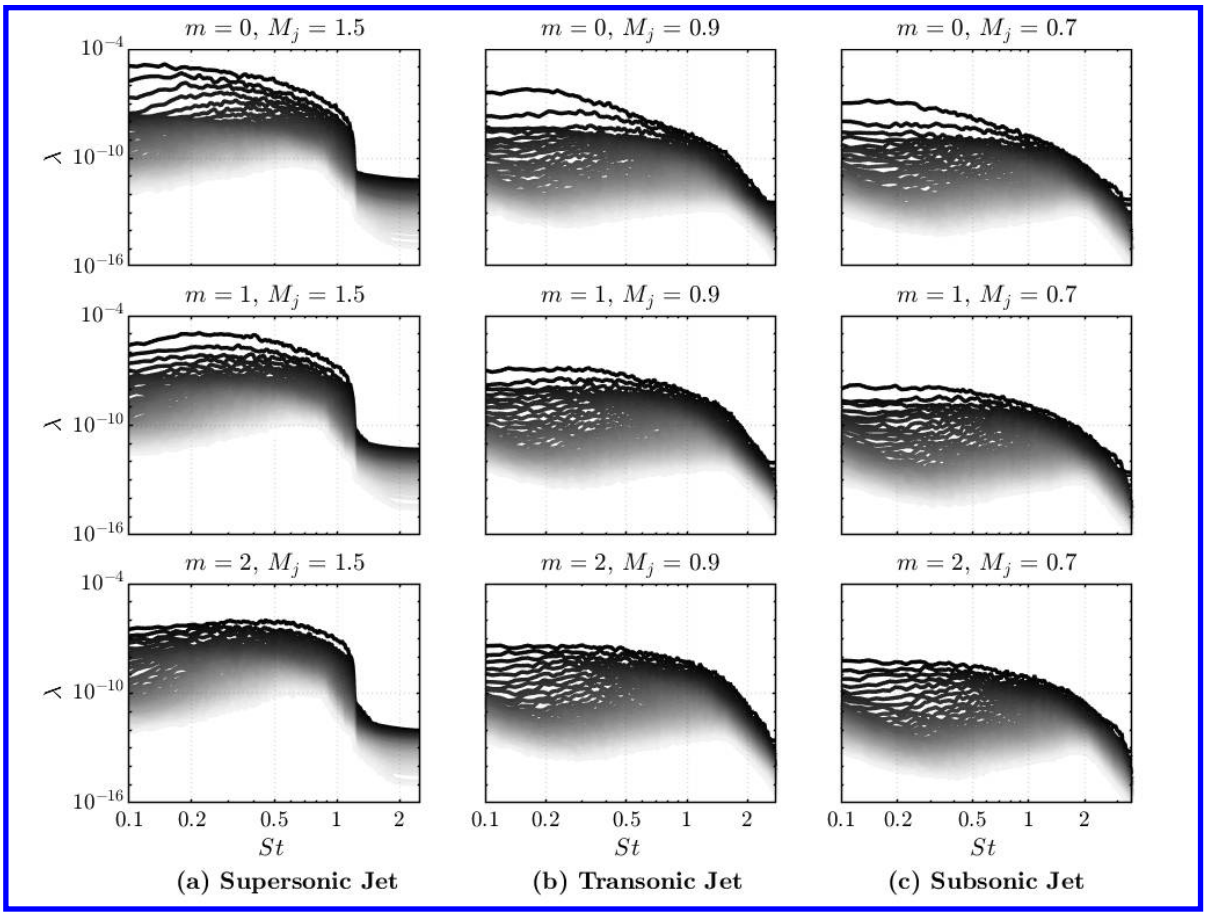

Fig. 3 SPOD eigenvalue spectra for the far-field focus region as defined in Eq. (12).

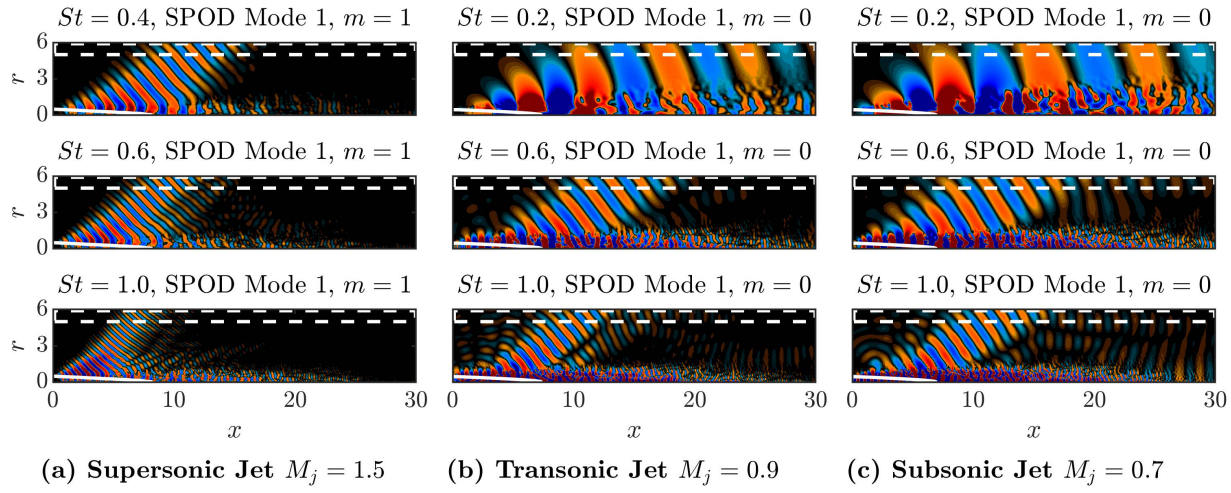

Fig. 4 Leading SPOD modes at peak frequencies (top row) , $St = 0.6$ (middle row) and for $St = 1.0$ (bottom row). The focus region is indicated by the dashed white box. White solid lines represent the edge of the potential core defined as $\bar{u}(x, r) = 0.95U_j$, where $\bar{u}$ is the mean axial velocity.

originate from the KH wavepacket and the Orr-type waves, respectively [21, 49]. The higher suboptimal modes of the transonic and subsonic jets (middle and bottom row of Fig. 5 (b) and (c)) exhibit upstream and sideline propagating

radiation. In section IV.B, this observation is addressed in more detail. Notably, very similar radiation patterns have been predicted by Jeun et al. [19] using resolvent analysis and global modes Schmidt et al. [24].

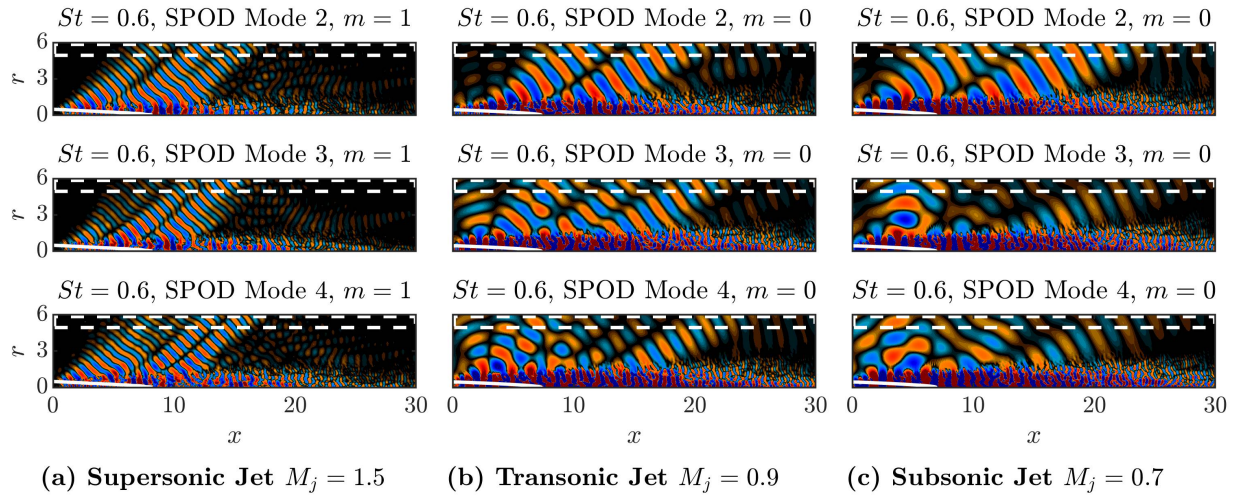

(a) **Supersonic Jet** $M_j = 1.5$ (b) **Transonic Jet** $M_j = 0.9$ (c) **Subsonic Jet** $M_j = 0.7$

Fig. 5 First, second and third suboptimal SPOD modes at $St = 0.60$. The focus region is indicated by the dashed white box. White solid lines represent the edge of the potential core defined as $\bar{u}(x, r) = 0.95U_j$, where $\bar{u}$ is the mean axial velocity.

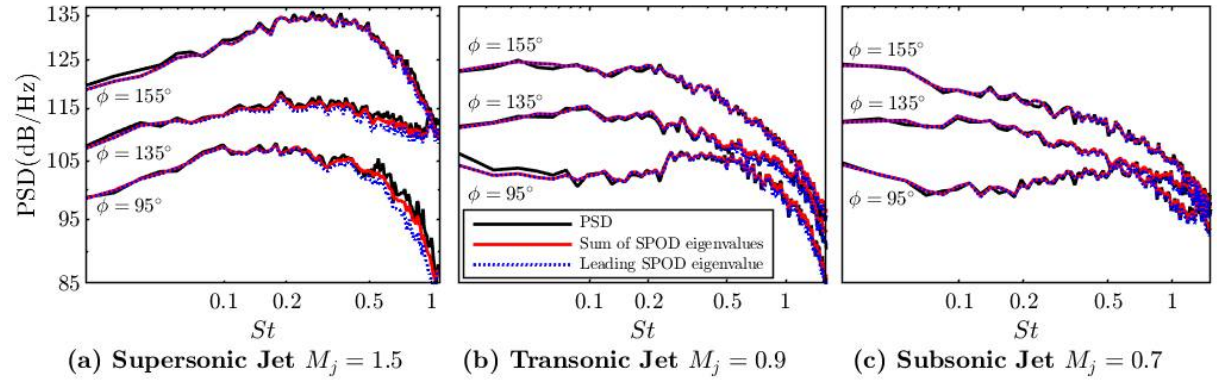

(a) **Supersonic Jet** $M_j = 1.5$ (b) **Transonic Jet** $M_j = 0.9$ (c) **Subsonic Jet** $M_j = 0.7$

Fig. 6 Comparison of PSD and SPOD spectra. Black lines represent the PSD, blue dotted lines represent the first SPOD mode and red lines represent the sum of all SPOD modes.

Next, we examine the dominant radiation patterns for different angles by introducing a new weighting function $W_f(x)$ that focuses on small boxes that are representative of specific angles,

$$W_f(x) = \begin{cases} 1 & \text{for } 5 \le r \le 6, x_f - 0.5 < x < x_f + 0.5, \quad \text{where} \quad x_f \in [0.5, 29.5], \\ 0 & \text{otherwise.} \end{cases} \tag{13}$$

The center of each box of height and width $\Delta x = 1.0$ is used to calculate the angle. The PSD and SPOD spectrum for different inlet jet angles are compared in Fig. 6. To facilitate direct comparison with PSD, the SPOD spectrum is normalized by the area of the box. The leading SPOD mode (blue dotted line) is able to predict the PSD (black lines) accurately, in particular at low frequencies. The total SPOD energy is obtained as the sum of all SPOD eigenvalues and shown as red lines. Only a marginal improvement of the comparison over the leading mode energy is observed. The energy contained in the leading SPOD mode is found to account for at least 90% of the total energy over all frequencies. This shows that the radiation to specific angles is dominated by a specific source. Another conclusion is that a rank-1 SPOD approximation yields an accurate model of the directional radiation.

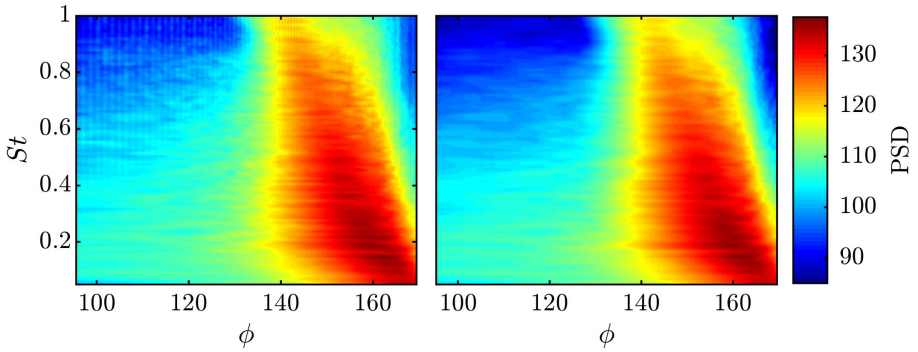

Fig. 7 PSD estimated from the (a) time series of the LES pressure data and (b) leading SPOD eigenvalue for $m = 0$ of the supersonic jet.

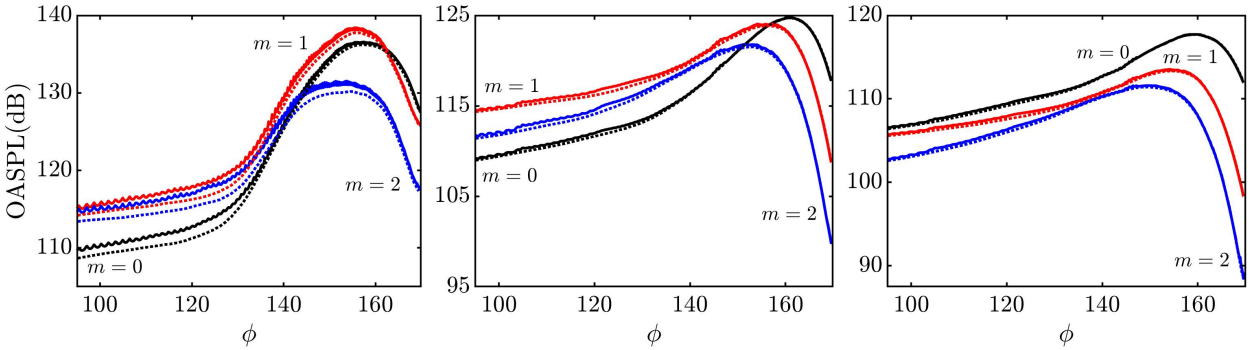

Fig. 8 Comparison between OASPL of the LES pressure data (solid lines) and leading SPOD eigenvalue (dotted lines): $m = 0$ (black) , $m = 1$ (red) and $m = 2$ (blue).

Fig. 7(b) shows the area-weighted eigenvalue of the leading SPOD mode as a function of frequency and inlet angle. The spectrum closely resembles the PSD of the raw pressure data shown in Fig. 7(a). For brevity, only the $m = 0$ component of the supersonic jet is shown, but similar results are found for all other cases. The OASPL calculated from the data and the area-weighted SPOD energy of the first mode are compared in Fig. 8(a-c). The rank-1 SPOD approximation follows the trend of the OASPL well. Jeun and Nicols [22] made similar observations for a rank-1 approximation based on resolvent analysis. For the two lower Mach number jets, the OASPL curves predicted by the rank-1 approximation are more accurate than in the supersonic case.

A. Superdirective radiation

The top row of Fig. 9 shows the leading SPOD modes focused on the locations of the peak OASPL (see Fig. 1 (a),(b) and (c)) and peak frequencies at the corresponding azimuthal wavenumbers. It is observed that the peak frequencies from the SPOD analysis and the peak PSD frequency coincide. This implies that the leading SPOD mode provides an accurate representation of the directive far-field radiation. superdirective beams that encompass the region being investigated are observed. For the lower Mach number jets, the acoustic beams originate from the end of the potential core, whereas this location appears to be shifted slightly upstream in the supersonic case. The observations made for $M_j = 0.9$ are in agreement with the findings of Bogey and Baily [50]. The superdirective radiation propagates at a steeper angle in the supersonic jet. The steeper propagation angle and upstream source location appear to cause a shift in the maximum directivity towards a lower jet inlet angle for the supersonic jet. Cavalieri et al. [10] argue that the azimuthal interference of the helical mode and the smaller spatial extent of the helical wavepackets cause this difference. The leading SPOD modes at $St = 0.8$ are shown in the bottom row of Fig 9. Multiple beams emanating

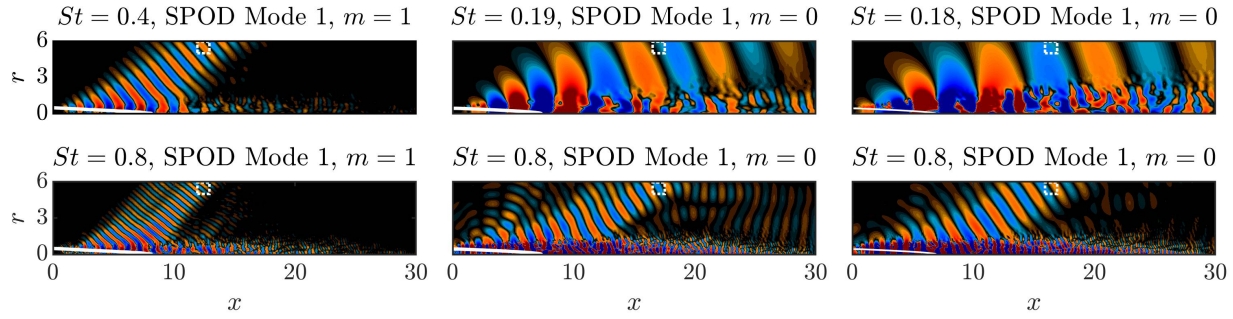

(a) Supersonic Jet $M_j = 1.5$ **(b) Transonic** Jet $M_j = 0.9$ **(c) Subsonic** Jet $M_j = 0.7$

Fig. 9 Leading SPOD modes at peak frequencies (top row) and for $St = 0.80$ (bottom row). The focus region is indicated by the dashed white box. White solid lines represent the edge of the potential core defined as $\bar{u}(x,r) = 0.95U_j$, where $\bar{u}$ is the mean axial velocity.

from different source locations are observed in the supersonic and the transonic jet. This decrease of directivity with increasing frequency is in agreement with the findings by Cavalieri et al. [10] and may be attributed to the decline of the dominance of the KH mechanism in this regime.

B. Noise Generated in the sideline direction

To understand the generation of jet noise in the sideline direction, we focus our attention to the dominant radiation patterns to angles $\phi < 135°$. These angles represent the region above the potential core. As before, we focus on the azimuthal wavenumber of the peak OASPL in that region (see Fig. 1). Fig. 10 depicts the leading SPOD modes for $\phi = 95°$. At the peak Strouhal numbers (top row of Fig. 10), upstream traveling radiation patterns are observed. The SPOD modes of the supersonic and transonic jets also reveal the presence of directive downstream radiation. Both the upstream and downstream radiation patterns originate from the same source location at the end of the potential core. Similar observation were made in a supersonic jet by Bogey and Gojon [51]. The leading modes at $St = 0.8$ (bottom row of Fig. 10) exhibit multi-directive radiation patterns that include upstream, sideline and downstream beams. In the supersonic case, the upstream radiation is clearly slaved to the much more energetic downstream radiation.

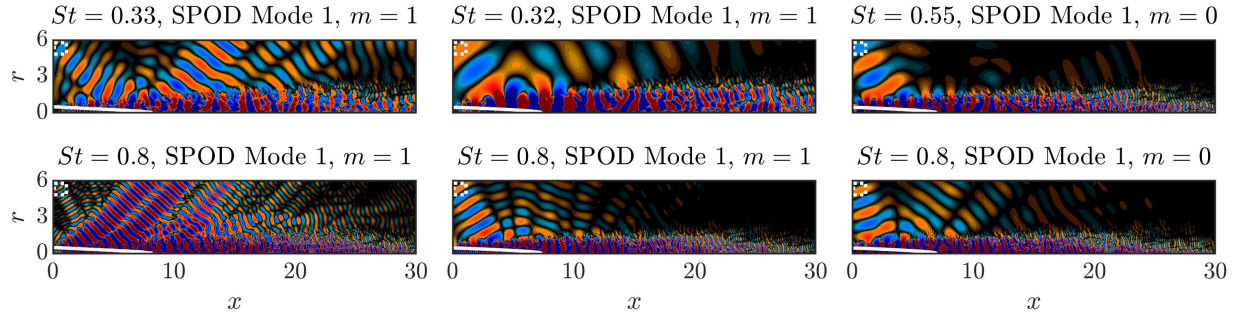

(a) Supersonic Jet $M_j = 1.5$ **(b) Transonic Jet** $M_j = 0.9$ **(c) Subsonic Jet** $M_j = 0.7$

Fig. 10 Leading SPOD modes at peak frequencies (top row) and for $St = 0.80$ (bottom row). The focus region is indicated by the dashed white box. White solid lines represent the edge of the potential core defined as $\bar{u}(x,r) = 0.95U_j$, where $\bar{u}$ is the mean axial velocity.

The sideline radiation perpendicular to the jet axis is investigated in Fig. 11. The focus region is chosen accordingly. Notably, the identified angles of $\phi = 112°$, $\phi = 129°$ and $\phi = 131°$ for the subsonic, transonic and supersonic jet, respectively, correspond to distinct frequency bands in Fig. 2. All modes also exhibit downstream radiation. For the supersonic jet, the downstream radiation is found considerably more energetic than the sideline beam. Similar to the

findings of Freund [52], these observations suggest that the sideline radiation is directly coupled with the dominant directive radiations, implying that both originate from the same source at the end of the potential core. For the higher frequency, $St = 0.8$, the source location is further upstream. This trend can be explained by the fact that the peak location of the KH wavepacket moves upstream with increasing frequency. The leading SPOD modes of the supersonic and the transonic jets at $St = 0.80$ (bottom row Fig. 11 (a) and (b)) show multi-directive radiation patterns.

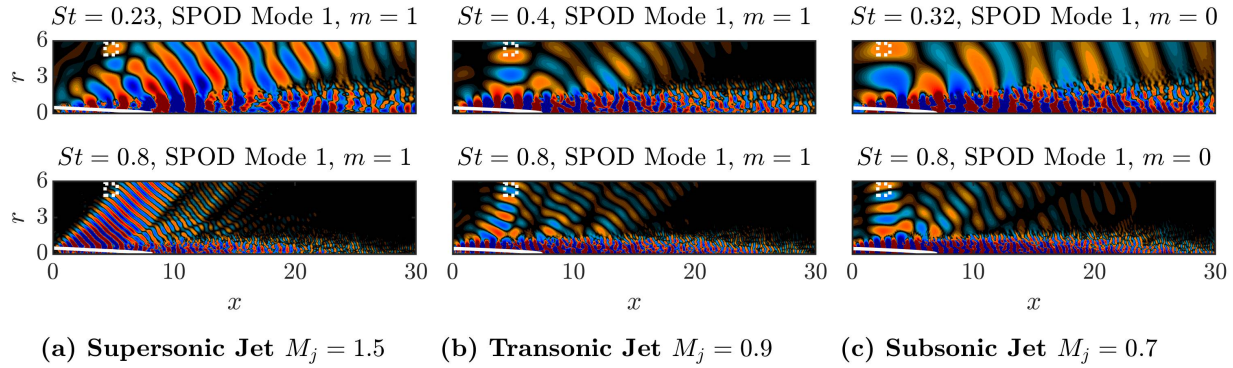

(a) Supersonic Jet $M_j = 1.5$ **(b) Transonic Jet $M_j = 0.9$** **(c) Subsonic Jet $M_j = 0.7$**

Fig. 11 Leading SPOD modes at peak frequencies (top row) and for $St = 0.80$ (bottom row). The focus region is indicated by the dashed white box. White solid lines represent the edge of the potential core defined as $\bar{u}(x, r) = 0.95U_j$, where $\bar{u}$ is the mean axial velocity.

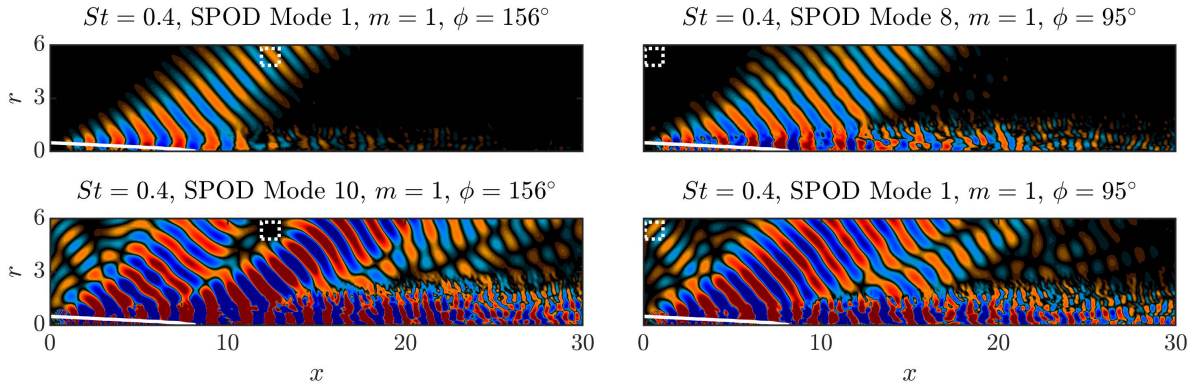

Fig. 12 Comparison of leading and suboptimal SPOD modes for the supersonic jet $M_j = 1.5$ at $St = 0.40$: mode 1 (top left) and mode 10 (bottom left) for $\phi = 156°$; mode 8 (top right) and mode 1 (bottom right) for $\phi = 95°$. The most similar modes were identified by visual inspection.

Next, we inspect the link between downstream and sideline radiation. In Fig. 12, the leading mode at $\phi = 156°$ is compared with a higher mode (lower energy) at $\phi = 95°$ and vice versa. The leading mode corresponding to the region of maximum directivity and the eighth mode at $\phi = 95°$ are observed to resemble each other. Both of these modes exhibit superdirective beams that propagate at the same angle and originate from a similar location in the shear-layer. The bottom row of Fig. 12 shows the tenth mode at $\phi = 156°$ and the leading mode at $\phi = 95°$. As before, close correspondence is found. This results clearly suggests that the sideline radiation is directly linked to the dominant downstream radiation pattern. Similar observations are found for the other cases. Combined, the observations made in the context of Figs. 9-12 strongly suggest that a single mechanism is responsible for the generation of noise towards the downstream and sideline directions. An important implication from a modeling perspective is that structures that are found to be dominant for a particular spatial weighting are recovered as suboptimal modes in the other. This mean that, if a sufficient number of SPOD modes is retained, the two SPOD basis span a similar space.

Fig. 13 aims at summarizing our results in a compact and interpretable way by relating the source location, radiation angle and peak frequency. First, the peak Strouhal number of the leading SPOD mode is selected for each ϕ, or far-field

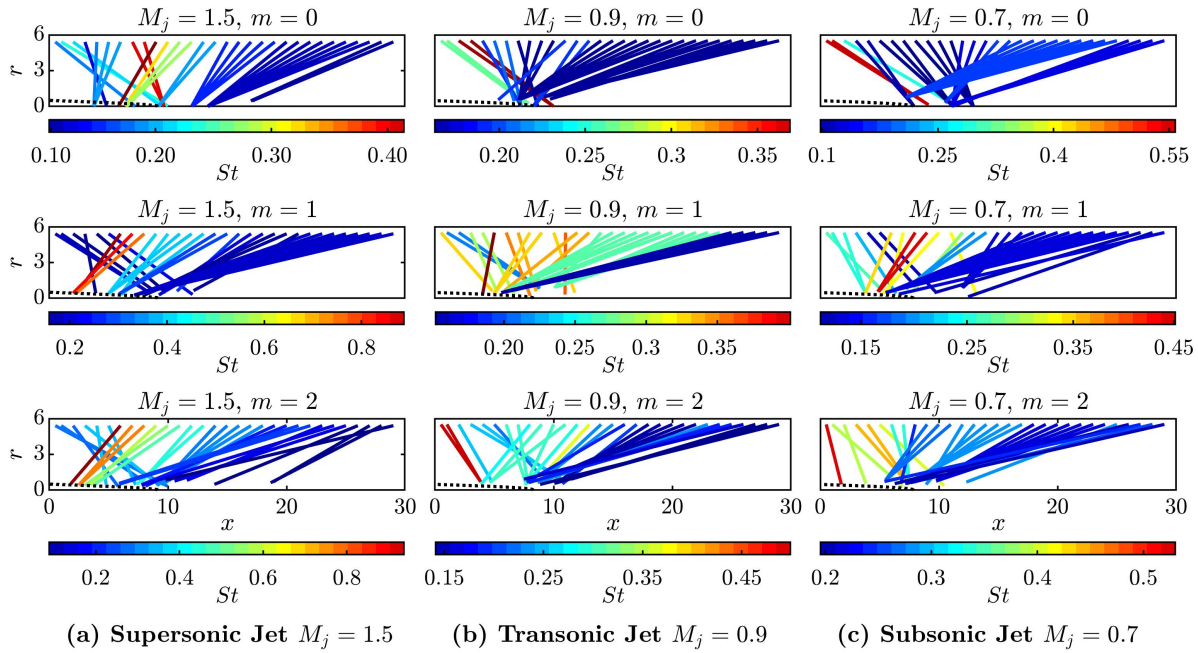

(a) Supersonic Jet $M_j = 1.5$ **(b) Transonic Jet $M_j = 0.9$** **(c) Subsonic Jet $M_j = 0.7$**

Fig. 13 Directivity plot obtained from directional SPOD analysis: straight lines connect far-field focus region to location of maximum absolute value of SPOD mode at peak frequency. Peak frequencies are indicated by false colors.

location. Each line then connects the far-field location to the point corresponding to the absolute maximum of the mode $\|\psi^{(1)}_{St_{peak}}\|_\infty$. This point serves as a proxy for the source location. False colors indicate the corresponding peak frequency. A few trends are observed. The primary source of the dominant downstream radiation appears to be located in the region surrounding the end of the potential core. Sideline radiation to low angles emanates from the jet shear-layer or the end of the potential core. In most cases, the sideline radiation appears to be slaved to the directive downstream radiation. In all cases the source location is in the vicinity of the jet axis ($r \approx 0$) or the lipline ($r \approx 0.5$), i.e., in the region where the Kelvin-Helmholtz wavepackets (inside the shear-layer) and Orr-type wavepackets (downstream of the potential core) dominate the dynamics of the jet. As observed earlier, the dominant superdirective radiation occurs at frequencies of $St \approx 0.2$, whereas higher frequencies are observed in the sideline direction.

V. Summary and conclusion

The first three azimuthal wavenumber components of supersonic, transonic, and subsonic jets are analyzed using spectral proper orthogonal decomposition with localized weighting. The dominant component is $m = 1$ for the supersonic jet and $m = 0$ for the subsonic case. In the transonic regime, $m = 1$ for $\phi \leq 150°$ is surpassed by $m = 0$ for $\phi > 150°$. In the sideline direction ($\phi \lesssim 130°$), the $m = 1$ and $m = 2$ components are relatively more important. For all cases, the frequency of the peak PSD in the $m = 0$ component occurs for $St \approx 0.2$. The SPOD analysis identifies a single directive beam at $\phi \approx 160°$ as the corresponding radiation pattern. The source of this superdirective beam is at the end of the potential core for low frequencies and in the shear-layer for higher frequencies. Suboptimal SPOD modes show multi-directive patterns that include radiation in the upstream and sideline directions. For the first few modes, a clear hierarchy is observed that directly relates the mode number to the number of beams. Additional data may further confirm this finding by improving convergence of the SPOD. Noise in the sideline direction is in most cases associated with higher frequencies. The SPOD modes reveal that the largest contributions to noise emissions in the sideline and downstream directions both take the form of acoustic beams that originate from the end of the potential core. The inspection of modes at different angles and suboptimal modes further underlines the notion that sideline and downstream radiation share the same source. A comparison of the SPOD spectra with the OASPL shows that the first SPOD eigenvalue accurately approximates the overall sound pressure over all angles. This implies that the

corresponding mode structure is the single largest contributor to directional noise. Despite the limited radial extend of the domain, the above observations strongly suggest a single source mechanism for turbulent jet noise in all directions. A possible source mechanism that was previously investigated in the context of wavepacket modeling by Cavalieri and Agarwal [53] is coherence decay. In particular, we propose a scenario in which the distortion of a coherent KH wavepacket gives rise to a multi-directive burst event. Future SPOD-based jet noise models may further benefit from the observation that both the dominant downstream and sideline radiation patters are part of a single SPOD basis.

References

[1] Crow, S. C., and Champagne, F., "Orderly structure in jet turbulence," *Journal of Fluid Mechanics*, Vol. 48, No. 3, 1971, pp. 547–591.

[2] Brown, G. L., and Roshko, A., "On density effects and large structure in turbulent mixing layers," *Journal of Fluid Mechanics*, Vol. 64, No. 4, 1974, pp. 775–816.

[3] Mollo-Christensen, E., "Jet noise and shear flow instability seen from an experimenter's viewpoint," 1967.

[4] Michalke, A., "Instability of a compressible circular free jet with consideration of the influence of the jet boundary layer thickness," 1977.

[5] Crighton, D., and Gaster, M., "Stability of slowly diverging jet flow," *Journal of Fluid Mechanics*, Vol. 77, No. 2, 1976, pp. 397–413.

[6] Tam, C. K., and Morris, P. J., "The radiation of sound by the instability waves of a compressible plane turbulent shear layer," *Journal of Fluid Mechanics*, Vol. 98, No. 2, 1980, pp. 349–381.

[7] Tam, C. K., and Burton, D. E., "Sound generated by instability waves of supersonic flows. Part 1. Two-dimensional mixing layers," *Journal of Fluid Mechanics*, Vol. 138, 1984, pp. 249–271.

[8] Crighton, D., and Huerre, P., "Shear-layer pressure fluctuations and superdirective acoustic sources," *Journal of Fluid Mechanics*, Vol. 220, 1990, pp. 355–368.

[9] Jordan, P., and Colonius, T., "Wave packets and turbulent jet noise," *Annual review of fluid mechanics*, Vol. 45, 2013, pp. 173–195.

[10] Cavalieri, A. V., Jordan, P., Colonius, T., and Gervais, Y., "Axisymmetric superdirectivity in subsonic jets," *Journal of fluid Mechanics*, Vol. 704, 2012, pp. 388–420.

[11] Tam, C., Golebiowski, M., and Seiner, J., "On the two components of turbulent mixing noise from supersonic jets," *Aeroacoustics conference*, 1996, p. 1716.

[12] Viswanathan, K., "Analysis of the two similarity components of turbulent mixing noise," *AIAA journal*, Vol. 40, No. 9, 2002, pp. 1735–1744.

[13] Viswanathan, K., "Aeroacoustics of hot jets," *Journal of Fluid Mechanics*, Vol. 516, 2004, pp. 39–82.

[14] Tam, C. K., Viswanathan, K., Ahuja, K., and Panda, J., "The sources of jet noise: experimental evidence," *Journal of Fluid Mechanics*, Vol. 615, 2008, pp. 253–292.

[15] Nichols, J. W., and Lele, S. K., "Global modes and transient response of a cold supersonic jet," *Journal of Fluid Mechanics*, Vol. 669, 2011, pp. 225–241.

[16] Gudmundsson, K., and Colonius, T., "Parabolized stability equation models for turbulent jets and their radiated sound," *15th AIAA/CEAS Aeroacoustics Conference (30th AIAA Aeroacoustics Conference)*, 2009, p. 3380.

[17] Rodriguez, D., Sinha, A., Brès, G., and Colonius, T., "Parabolized Stability Equation models in turbulent supersonic jets," *18th AIAA/CEAS Aeroacoustics Conference (33rd AIAA Aeroacoustics Conference)*, 2012, p. 2117.

[18] Rodriguez, D., Sinha, A., Bres, G. A., and Colonius, T., "Acoustic field associated with parabolized stability equation models in turbulent jets," *19th AIAA/CEAS Aeroacoustics Conference*, 2013, p. 2279.

[19] Jeun, J., Nichols, J. W., and Jovanović, M. R., "Input-output analysis of high-speed axisymmetric isothermal jet noise," *Physics of Fluids*, Vol. 28, No. 4, 2016, p. 047101.

[20] Jeun, J., and Nichols, J. W., "Wavepacket modeling of turbulent jet noise generation using input-output analysis," *23rd AIAA/CEAS Aeroacoustics Conference*, 2017, p. 3378.

[21] Schmidt, O. T., Towne, A., Rigas, G., Colonius, T., and Brès, G. A., "Spectral analysis of jet turbulence," *Journal of Fluid Mechanics*, Vol. 855, 2018, pp. 953–982.

[22] Jeun, J., and Nichols, J. W., "Non-compact sources of sound in high-speed turbulent jets using input-output analysis," *2018 AIAA/CEAS Aeroacoustics Conference*, 2018, p. 3467.

[23] Jeun, J., and Nichols, J. W., "Input-output analysis of Mach 0.9 jet noise," *arXiv preprint arXiv:1806.09280*, 2018.

[24] Schmidt, O., Towne, A., Colonius, T., Jordan, P., Jaunet, V., Cavalieri, A. V., and Bres, G. A., "Super-and multi-directive acoustic radiation by linear global modes of a turbulent jet," *22nd AIAA/CEAS Aeroacoustics Conference*, 2016, p. 2808.

[25] Towne, A., Schmidt, O. T., and Colonius, T., "Spectral proper orthogonal decomposition and its relationship to dynamic mode decomposition and resolvent analysis," *Journal of Fluid Mechanics*, Vol. 847, 2018, pp. 821–867.

[26] Rigas, G., Schmidt, O. T., Colonius, T., and Bres, G. A., "One Way Navier-Stokes and resolvent analysis for modeling coherent structures in a supersonic turbulent jet," *23rd AIAA/CEAS Aeroacoustics Conference*, 2017, p. 4046.

[27] Tam, C. K., and Hu, F. Q., "On the three families of instability waves of high-speed jets," *Journal of Fluid Mechanics*, Vol. 201, 1989, pp. 447–483.

[28] Schmidt, O. T., and Schmid, P. J., "A conditional space–time POD formalism for intermittent and rare events: example of acoustic bursts in turbulent jets," *Journal of Fluid Mechanics*, Vol. 867, 2019.

[29] Towne, A., Cavalieri, A. V., Jordan, P., Colonius, T., Schmidt, O., Jaunet, V., and Brès, G. A., "Acoustic resonance in the potential core of subsonic jets," *Journal of Fluid Mechanics*, Vol. 825, 2017, pp. 1113–1152.

[30] Schmidt, O. T., Towne, A., Colonius, T., Cavalieri, A. V., Jordan, P., and Brès, G. A., "Wavepackets and trapped acoustic modes in a turbulent jet: coherent structure eduction and global stability," *Journal of Fluid Mechanics*, Vol. 825, 2017, pp. 1153–1181.

[31] Papamoschou, D., "Wavepacket modeling of the jet noise source," *International Journal of Aeroacoustics*, Vol. 17, No. 1-2, 2018, pp. 52–69.

[32] Taira, K., Brunton, S. L., Dawson, S. T., Rowley, C. W., Colonius, T., McKeon, B. J., Schmidt, O. T., Gordeyev, S., Theofilis, V., and Ukeiley, L. S., "Modal analysis of fluid flows: An overview," *Aiaa Journal*, 2017, pp. 4013–4041.

[33] Rowley, C. W., and Dawson, S. T., "Model reduction for flow analysis and control," *Annual Review of Fluid Mechanics*, Vol. 49, 2017, pp. 387–417.

[34] Lumley, J. L., "The structure of inhomogeneous turbulent flows," *Atmospheric turbulence and radio wave propagation*, 1967.

[35] Lumley, J. L., *Stochastic tools in turbulence*, Courier Corporation, 2007.

[36] Sirovich, L., "Turbulence and the dynamics of coherent structures. I. Coherent structures," *Quarterly of applied mathematics*, Vol. 45, No. 3, 1987, pp. 561–571.

[37] Glauser, M. N., Leib, S. J., and George, W. K., "Coherent structures in the axisymmetric turbulent jet mixing layer," *Turbulent Shear Flows 5*, Springer, 1987, pp. 134–145.

[38] Citriniti, J., and George, W. K., "Reconstruction of the global velocity field in the axisymmetric mixing layer utilizing the proper orthogonal decomposition," *Journal of Fluid Mechanics*, Vol. 418, 2000, pp. 137–166.

[39] Jung, D., Gamard, S., and George, W. K., "Downstream evolution of the most energetic modes in a turbulent axisymmetric jet at high Reynolds number. Part 1. The near-field region," *Journal of Fluid Mechanics*, Vol. 514, 2004, pp. 173–204.

[40] Welch, P., "The use of fast Fourier transform for the estimation of power spectra: a method based on time averaging over short, modified periodograms," *IEEE Transactions on audio and electroacoustics*, Vol. 15, No. 2, 1967, pp. 70–73.

[41] Brès, G. A., and Lele, S. K., "Modelling of jet noise: a perspective from large-eddy simulations," *Philosophical Transactions of the Royal Society A*, Vol. 377, No. 2159, 2019, p. 20190081.

[42] Brès, G. A., Jordan, P., Jaunet, V., Le Rallic, M., Cavalieri, A. V., Towne, A., Lele, S. K., Colonius, T., and Schmidt, O. T., "Importance of the nozzle-exit boundary-layer state in subsonic turbulent jets," *Journal of Fluid Mechanics*, Vol. 851, 2018, pp. 83–124.

[43] Brès, G. A., Ham, F. E., Nichols, J. W., and Lele, S. K., "Unstructured large-eddy simulations of supersonic jets," *AIAA journal*, 2017, pp. 1164–1184.

[44] Juve, D., Sunyach, M., and Comte-Bellot, G., "Filtered azimuthal correlations in the acoustic far field of a subsonic jet," *AIAA Journal*, Vol. 17, No. 1, 1979, pp. 112–113.

[45] Arndt, R. E., Long, D., and Glauser, M. N., "The proper orthogonal decomposition of pressure fluctuations surrounding a turbulent jet," *Journal of Fluid Mechanics*, Vol. 340, 1997, pp. 1–33.

[46] Cavalieri, A. V., Jordan, P., Agarwal, A., and Gervais, Y., "Jittering wave-packet models for subsonic jet noise," *Journal of Sound and Vibration*, Vol. 330, No. 18-19, 2011, pp. 4474–4492.

[47] Tinney, C., and Jordan, P., "The near pressure field of co-axial subsonic jets," *Journal of Fluid Mechanics*, Vol. 611, 2008, pp. 175–204.

[48] Nekkanti, A., and Schmidt, O., "Flow Field Reconstruction and Filtering Using Spectral Proper Orthogonal Decomposition," *Bulletin of the American Physical Society*, 2019.

[49] Tissot, G., Zhang, M., Lajús, F. C., Cavalieri, A. V., and Jordan, P., "Sensitivity of wavepackets in jets to nonlinear effects: the role of the critical layer," *Journal of Fluid Mechanics*, Vol. 811, 2017, pp. 95–137.

[50] Bogey, C., and Bailly, C., "An analysis of the correlations between the turbulent flow and the sound pressure fields of subsonic jets," *Journal of Fluid Mechanics*, Vol. 583, 2007, pp. 71–97.

[51] Bogey, C., and Gojon, R., "Feedback loop and upwind-propagating waves in ideally expanded supersonic impinging round jets," *Journal of Fluid Mechanics*, Vol. 823, 2017, pp. 562–591.

[52] Freund, J. B., "Noise sources in a low-Reynolds-number turbulent jet at Mach 0.9," *Journal of Fluid Mechanics*, Vol. 438, 2001, pp. 277–305.

[53] Cavalieri, A. V. G., and Agarwal, A., "Coherence decay and its impact on sound radiation by wavepackets," *Journal of Fluid Mechanics*, Vol. 748, 2014, pp. 399–415.